THE GEOLOGICAL SOCIETY OF AMERICA®

Zinc isotope evidence for intensive magmatism immediately before the end-Permian mass extinction

Sheng-Ao Liu[1]*, Huaichun Wu[2]*, Shu-zhong Shen[3], Ganqing Jiang[4], Shihong Zhang[2], Yiwen Lv[1], Hua Zhang[3], and Shuguang Li[1]

[1]State Key Laboratory of Geological Processes and Mineral Resources, China University of Geosciences, Beijing 100083, China
[2]State Key Laboratory of Biogeology and Environmental Geology, China University of Geosciences, Beijing 100083, China
[3]State Key Laboratory of Palaeobiology and Stratigraphy, Nanjing Institute of Geology and Palaeontology, Nanjing 210008; Centre of Integrated Science and Education for Evolution and Environment, Nanjing University, Nanjing 210023, China
[4]Department of Geoscience, University of Nevada,Las Vegas, Nevada 89154, USA

ABSTRACT

The end-Permian extinction is typically ascribed to massive volcanic eruptions, but direct geochemical evidence linking the two independent events is generally lacking. Zinc is an important micronutrient of marine phytoplanktons, and Zn isotope (δ^{66}Zn) ratios of seawater are markedly higher than those of volcanic rocks and riverine waters. We conducted high-resolution Zn concentration and Zn isotope analyses on carbonate rocks across the Permian-Triassic boundary (PTB) in the Meishan section of south China. An abrupt increase of Zn concentration and a concomitant 0.5‰ decrease in δ^{66}Zn occur ~35 k.y. before the mass extinction and carbon isotope (δ^{13}C) minima. Mass balance calculation demonstrates that a 0.5‰ negative shift in δ^{66}Zn within thousands of years requires rapid and massive input of isotopically light Zn from volcanic ashes, hydrothermal inputs, and/or extremely fast weathering of large igneous provinces. A positive δ^{66}Zn shift of as much as 1.0‰ following the mass extinction demonstrates that primary productivity recovered and reached a maximum in fewer than 360 k.y. Our finding provides insights into the marine Zn cycling across the PTB and clarifies the temporal relationship and duration of events, including intensive volcanism, carbon isotope excursion, mass extinction, and widespread ocean anoxia.

INTRODUCTION

The end-Permian mass extinction (EPME; 251.9 Ma) is characterized by abrupt disappearances of more than 90% of marine and 75% of terrestrial species and represents the greatest loss of biodiversity in the history of life (Erwin, 2006). This catastrophic biotic event is associated with prominent perturbations of the global carbon cycle (Korte and Kozur, 2010; Shen et al., 2013) and substantial paleoclimate-paleoceanographic changes, including fast global warming (Joachimski et al., 2012; Sun et al., 2012), ocean acidification (Payne et al., 2010; Garbelli et al., 2017), and widespread water-column anoxia and/or euxinia (Grice et al., 2005; Cao et al., 2009; Brennecka et al., 2011; Whiteside and Grice, 2016). The trigger of these events is typically linked to intensive volcanic eruptions represented by the Siberian Traps (Russia), the largest continental flood basalt province in the geological record (Reichow et al., 2009). High-precision U-Pb ages from Permian–Triassic strata in south China and volcanic rocks of the Siberian Traps (Shen et al., 2011; Burgess et al., 2014; Burgess and Bowring, 2015) support the synchrony of the mass extinction and volcanic eruptions and intrusions, but the timing of geochemical changes in the ocean relative to extinction, and the role of volcanism in triggering these changes, are not fully constrained; these require additional information to confirm, particularly data from new proxy records.

Zinc isotopes provide a means for investigating paleoceanographic changes (Maréchal et al., 2000; Kunzmann et al., 2013) that may help to clarify the causal link between events across the end-Permian mass extinction interval. Zinc is an important micronutrient used in enzymes by many marine phytoplanktons (Hendry and Andersen, 2013; Conway and John, 2014). Utilization of Zn by photosynthetic organisms commonly results in a shallow to deep ocean Zn gradient, with higher Zn concentration toward the deeper ocean (Conway and John, 2014). Bioassimilation tends to utilize light Zn isotopes, resulting in enrichment of heavy Zn isotopes (or higher δ^{66}Zn relative to the Johnson Matthey Zn standard solution JMC 3–0749L) in surface oceans that could be recorded by trace Zn incorporated into the crystal lattices of carbonate minerals (Maréchal et al., 2000; Little et al., 2014). Culture experiments demonstrated that δ^{66}Zn values of intercellular Zn in phytoplankton are as much as 0.8‰ lower than that of the dissolved phase (Peel et al., 2009). Due to preferential uptake and removal of light Zn isotopes by primary producers, the average δ^{66}Zn value of modern surface seawater (~0.9‰; Maréchal et al., 2000; Little et al., 2014) is significantly higher than those of volcanic rocks (~0.28‰; Chen et al., 2013) and riverine waters (~0.33‰; Little et al., 2014). Although deep seawater has lower δ^{66}Zn values than that of surface water, the average deep-water δ^{66}Zn value of ~0.51‰ (Little et al., 2014) is also higher than that of igneous rocks (~0.28‰). On this basis we hypothesize that if a fast increase of Zn from volcanic ashes, hydrothermal fluids, and enhanced weathering of large igneous provinces (LIPs) happened prior to the mass extinction, a significant drop in δ^{66}Zn of ocean water would be recorded in carbonate rocks. To test this hypothesis, we have conducted a detailed study on the Zn concentration and Zn isotope changes of carbonate rocks across the Permian-Triassic boundary (PTB) in Meishan, south China.

GEOLOGICAL BACKGROUND AND SAMPLING

The Meishan section in Changxing county, south China (Fig. 1), is the stratotype section for the Changhsingian Stage (see the GSA Data Repository[1]) and hosts the Global Stratotype Section and Point (GSSP) for the PTB and the Wuchiapingian-Changhsingian boundary (Yin et al., 2001; Jin et al., 2006). The Late Permian Changhsing Formation in this section is composed of micritic limestone and the overlying Yinkeng Formation consists of parallel-laminated calcareous mudstone with intercalations of thin-bedded limestone (Fig. 2). These rocks were deposited in middle-upper slope environments in the tropical area of eastern Paleotethys (Fig. 1). The EPME interval has been identified between the top

*E-mails: lsa@cugb.edu.cn; whcgeo@cugb.edu.cn

[1]GSA Data Repository item 2017099, sampling section, methods, Figures DR1–DR4, and Tables DR1–DR5, is available online at http://www.geosociety.org/datarepository/2017/ or on request from editing@geosociety.org.

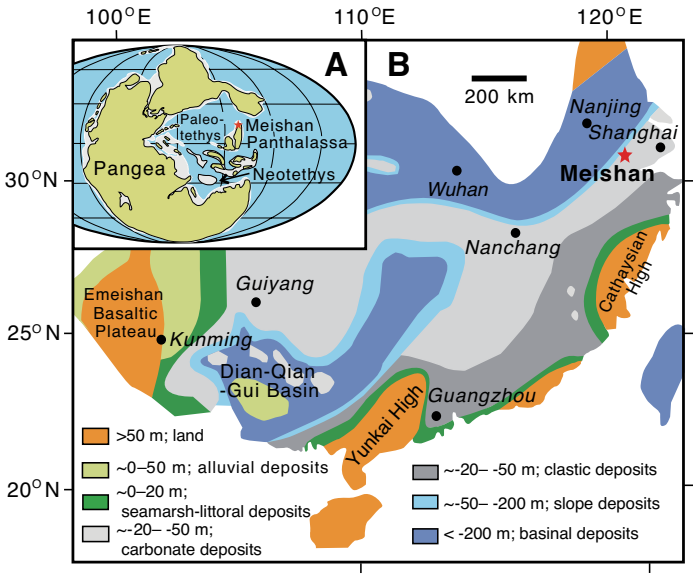

Figure 1. A: Paleogeographic location of the Meishan (south China) section during the Permian–Triassic transition (modified from Ziegler et al., 1997). B: Late Permian paleogeographic configuration of south China showing the location of the Meishan section (red star) (after Shen et al. 2011).

of bed 24e and bed 28 (Fig. 2; Shen et al., 2011). This section provides the most detailed record across the end-Permian mass extinction with precise U-Pb ages and astrochronology constraints (Shen et al., 2011; Wu et al., 2013; Burgess et al., 2014). Limestone samples (n = 65) were collected from a 20-m-thick drill core (M1; beds 19–37) across the PTB at the Meishan section (Cao et al., 2009; Tables DR1 and DR2 in the Data Repository).

ANALYTICAL METHODS

Major and trace elements and carbon and oxygen isotopes were analyzed across the PTB (for methods, see the Data Repository). To obtain a reliable Zn isotope signature, a leaching procedure modified from previously established methods (Pichat et al., 2003) was designed to extract the carbonate fraction of petrographically screened samples (details in the Data Repository). Prior to carbonate leaching, hydrosoluble salts and exchangeable fractions on clays (e.g., adsorbed) were removed using Milli-Q water and 1 M ammonium acetate. The carbonate fraction was then leached with 2 steps of 0.05 M acetic acid in a thermostat at 65 °C, followed by centrifugation, filtration, and purification. Zinc isotopic ratios were measured using a Neptune Plus multicollector–inductively coupled plasma–mass spectrometer. The whole-procedural reproducibility of Zn isotope analysis of standards and carbonate rocks is better than ±0.10‰ (2σ).

RESULTS

Carbon isotope data from the Meishan section show a sharp negative shift down to –3.2‰ 5 cm below bed 25; this is consistent with previously published $\delta^{13}C_{carb}$ data from the same section (Shen et al., 2013; Burgess et al., 2014; Fig. 2; Table DR1). The temporal $\delta^{66}Zn$ variations across the PTB can be divided into four stages (Fig. 2). Stage S1 (beds 19–24b) has an average $\delta^{66}Zn$ value of 0.83‰ ± 0.14‰ (2 sd) covering the latest Permian Changhsing Formation. A rapid 0.5‰ decrease in $\delta^{66}Zn$ from ~0.83‰ down to 0.34‰ ± 0.18‰ (2 sd) starts at bed 24c, 83 cm below the PTB, or ~35 k.y. before the mass extinction (stage S2). This negative $\delta^{66}Zn$ shift is accompanied by an increase in Zn concentration (by more than one order of magnitude) and within the gradual decline of the $\delta^{13}C$ excursion from the middle part of bed 23, but significantly

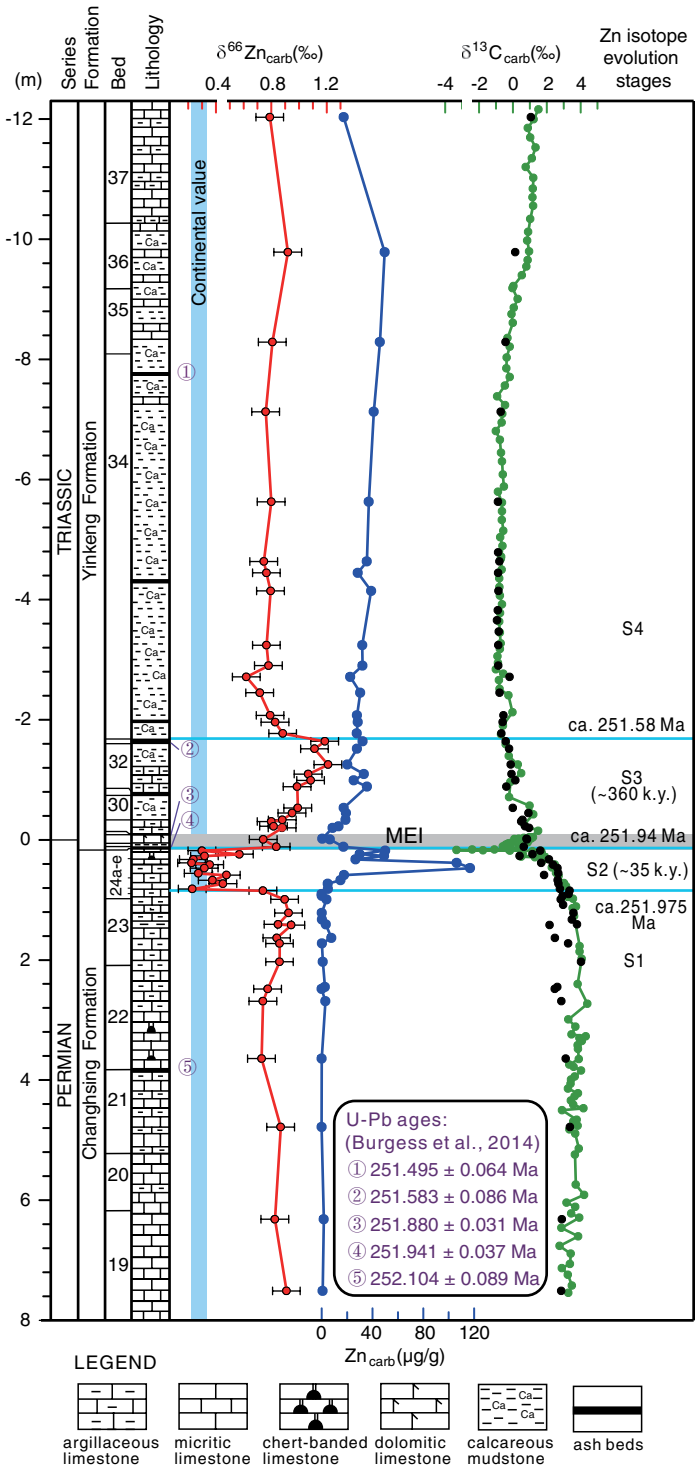

Figure 2. Lithostratigraphy and Zn isotope, Zn concentration, and carbon isotope variations across the Permian-Triassic boundary in the Meishan section (MEI), south China. Note that the negative shift in $\delta^{66}Zn$ slightly predates the sharp negative $\delta^{13}C$ excursion. The durations (in k.y.) of Zn isotope evolution stages S1–S4 are summarized from Wu et al. (2013) and Burgess et al. (2014). The $\delta^{13}C$ data are from Shen et al. (2011) (green dots) and this study (black dots). Error bars of $\delta^{66}Zn$ data correspond to 95% confidence level (≤0.1‰) determined from replicated analyses (GSA Data Repository; see footnote 1).

predates the $\delta^{13}C$ minima at the top of bed 24e (Fig. 2). Across the PTB, $\delta^{66}Zn$ increases to 1.21‰ in bed 32 of the Yinkeng Formation (stage S3), followed by a decrease to stable background values of 0.78‰ ± 0.14‰ (2 sd) from bed 34–37 (stage S4).

DISCUSSION

Data Evaluation and Reliability

Several lines of evidence suggest that the measured $\delta^{66}Zn$ values record a primary seawater signature. First, the $\delta^{66}Zn$ shift is not related to changes in precipitation rate or diagenesis indicated by Sr/Ca or $\delta^{18}O$ (Fig. 3A; Fig. DR1). Second, $\delta^{66}Zn$ values do not covary with concentrations of major oxides (e.g., SiO_2 and Al_2O_3; Fig. 3B; Fig. DR2), indicating that the $\delta^{66}Zn$ shift did not result from adsorption of Zn onto silicate or clay minerals. The samples with a high Zn concentration but low $\delta^{66}Zn$ do not show high bulk Al_2O_3, suggesting negligible siliciclastic-derived Zn. Third, the insoluble residues have almost constant $\delta^{66}Zn$ values of 0.3‰–0.4‰ (Table DR2) that are similar to the average crustal $\delta^{66}Zn$ value of 0.33‰ but differ from values of dissolved carbonates for most samples. The crust-like $\delta^{66}Zn$ values of insoluble residues also indicate negligible Zn isotope fractionation associated with Zn adsorption into Fe and Mn hydroxides, clays, or other colloids. Furthermore, the large temporal $\delta^{66}Zn$ variations are not likely to have been caused by increase of seawater temperature from bed 26 and across the PTB (Joachimski et al., 2012), because an increase of 8–10 °C in seawater temperature changes carbonate-seawater Zn isotope fractionation by <~0.1‰ (Fujii et al., 2011), and it significantly postdated the onset of the negative excursion of $\delta^{66}Zn$ at bed 24c (Fig. 2). Thus, we believe that the large temporal $\delta^{66}Zn$ variations most likely record the evolution of seawater Zn isotope composition from the latest Permian to the Early Triassic.

Evidence for Intense Magmatism Immediately Before the Extinction

At stage S1 (prior to 251.975 Ma), $\delta^{66}Zn$ values (~0.83‰) are higher than average riverine input (~0.33‰), but comparable with the average $\delta^{66}Zn$ value of the modern surface ocean (~0.9‰; Little et al., 2014), indicating that the seawater was enriched in ^{66}Zn due to preferential biological uptake of ^{64}Zn, as observed in the modern ocean (Maréchal et al., 2000). The abrupt negative $\delta^{66}Zn$ shift down to 0.34‰ at stage S2 (251.975–251.941 Ma) could be caused by shutdown of the primary productivity or a rapid increase of Zn from ^{66}Zn-depleted external sources. A complete shutdown of the ecosystem can be excluded because the negative $\delta^{66}Zn$ excursion occurs in fossiliferous strata (beds 24c–24e) indicative of a highly diverse ecosystem prior to the mass extinction (e.g., Shen et al., 2011; Fig. 2). External zinc input is required from sources that have $\delta^{66}Zn$ at least 0.5‰ lower than that of the preexisting surface seawater. Volcanic rocks and riverine inputs with average $\delta^{66}Zn$ values of ~0.3‰ are the most probable candidates. If the Zn fluxes and/or sinks and isotope compositions of the end-Permian ocean are similar to those of the modern ocean (Little et al., 2014), mass balance calculation shows that even with riverine input ($\delta^{66}Zn \approx 0.33‰$) 10 times larger than the modern drainage system and a shutdown of biological Zn uptake, a 0.5‰ negative shift in $\delta^{66}Zn$ would take at least 20 k.y. (calculations in Data Repository). However, the rapid negative $\delta^{66}Zn$ shift occurs within a ≤3 cm interval that represents <1.5 ± 1.0 k.y. (Wu et al., 2013; Burgess et al., 2014), indicating that weathering alone is unlikely to explain the rapid change in $\delta^{66}Zn$. Thus, we interpret that the initial, abrupt decline in $\delta^{66}Zn$ right before the EPME was most likely caused by fast input of a total of 8.06×10^{12} kg of ^{66}Zn-depleted zinc into the ocean from volcanic ashes, hydrothermal fluids, and/or extremely fast weathering of fresh LIPs.

Enhanced CO_2-driven weathering input in response to fast volcanic eruptions (Algeo and Twitchett, 2010) certainly contributed to the sustained lower $\delta^{66}Zn$ values up to the PTB. This is consistent with the fact that the negative $\delta^{66}Zn$ shift predates the sharp $\delta^{13}C$ excursion (Fig. 2). In the modern ocean, the residence time of Zn (~50 k.y.; Shiller and Boyle, 1985) is approximately half of the carbon residence time. The shorter residence time of Zn explains the faster (than carbon) change of Zn concentration and Zn isotopes in response to volcanism and weathering.

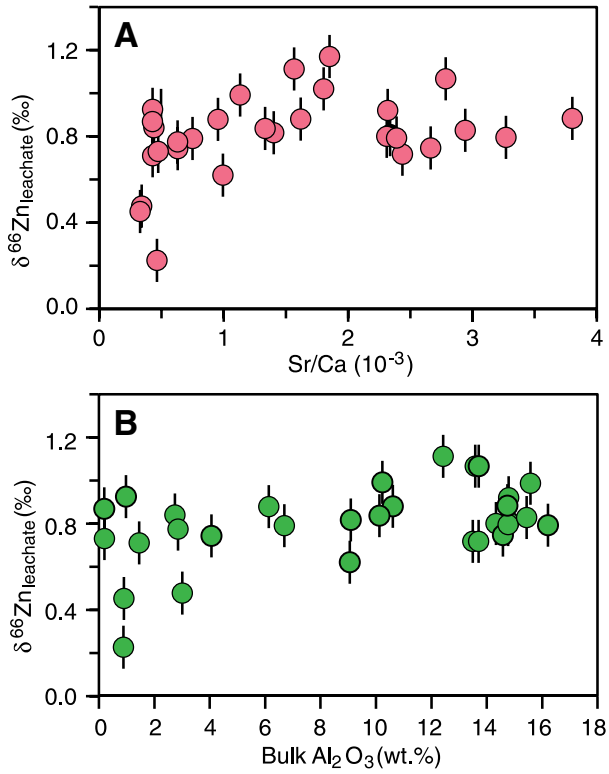

Figure 3. A: Cross-plots of $\delta^{66}Zn$ versus Sr/Ca ratio of carbonate samples from the Meishan (south China) section. B: Cross-plots of $\delta^{66}Zn$ versus Al_2O_3 contents. The lack of $\delta^{66}Zn$-Sr/Ca and $\delta^{66}Zn$-Al_2O_3 covariation suggests that the observed temporal $\delta^{66}Zn$ variations are not caused by diagenesis or contamination from clay minerals or other silicates. Original data are included in Tables DR2, DR4, and DR5 (see footnote 1).

Ocean Environmental Changes After Mass Extinction

The positive shift of up to ~1.0‰ in $\delta^{66}Zn$, from 0.34‰ to 1.21‰ across the PTB (stage S3; Fig. 2), may record high primary productivity following the EPME (Fig. DR4; Grice et al., 2005), consistent with the resurgence and expansion of microbialites shortly after the mass extinction (Kershaw et al., 2012). A strong primary biological pump driven by high nutrient input in response to warming and enhanced weathering must have been developed long before the reestablishment of stable, complex ecosystems; that did not happen until a few million years later (Algeo and Twitchett, 2010). Increase of primary productivity may have led to expanded ocean anoxia that may have also partially contributed to the positive shift in $\delta^{66}Zn$, because burial of sulfides (e.g., FeS_2 and ZnS) preferentially removes ^{64}Zn (Fujii et al., 2011; Vance et al., 2016). Widespread anoxia, well established during the end-Permian and Early Triassic (Brennecka et al., 2011), would have drastically changed the oxic burial flux of zinc globally. The return of $\delta^{66}Zn$ to stable background values (stage 4; Fig. 2) identical to pre-extinction $\delta^{66}Zn$ after ca. 251.58 Ma suggests that primary production reached its maximum within ~360 k.y. after the mass extinction.

CONCLUSION

The observed patterns of $\delta^{66}Zn$ and Zn concentration across the PTB in Meishan, south China, provide a unique data set that clarifies the temporal relationship of events across the EPME. The rapid negative $\delta^{66}Zn$ shift from 0.84‰ down to a near crustal value of 0.34‰ provides clear evidence for the increase of isotopically light Zn input from volcanic ashes, hydrothermal fluids, and/or extremely fast weathering of fresh LIPs ~35 k.y. before the EPME. The positive $\delta^{66}Zn$ shift from a near crustal value of 0.34‰ to 1.21‰ across the PTB may record fast recovery of

primary production following the mass extinction. An increase of primary production, possibly fed by enhanced nutrient supply and promoted by vacant ecological niches favored by microorganisms (e.g., cyanobacteria and algae), may have resulted in eutrophication, significant ocean stratification, and widespread ocean anoxia that significantly delayed the recovery of diversified ecosystems. The Zn isotope and Zn concentration records from the Meishan section may also serve as a useful reference to compare the temporal relationship of events across the PTB in disparate sections, where other chemostratigraphic and/or paleontologic records are poorly preserved.

ACKNOWLEDGMENTS

We thank Karl Krainer and Tianshui Yang for suggestions on the manuscript, and Chenxiao Liu for assistance in the lab. We also thank Judith T. Parrish, Kliti Grice, Quentin Crowley, and Seth D. Burgess for very helpful comments that significantly improved the final manuscript. This work is supported by the National Natural Science Foundation of China (grants 41473017, 41422202, 41290260, and 41273081), the Fundamental Research Funds for the Central Universities (grants 2652014068 and 2652015297) and the Strategic Priority Research Program (B) of the Chinese Academy of Sciences (grant XDB18000000).

REFERENCES CITED

Algeo, T.J., and Twitchett, R.J., 2010, Anomalous Early Triassic sediment fluxes due to elevated weathering rates and their biological consequences: Geology, v. 38, p. 1023–1026, doi:10.1130/G31203.1.

Brennecka, G.A., Herrmann, A.D., Algeo, T.J., and Anbar, A.D., 2011, Rapid expansion of oceanic anoxia immediately before the end-Permian mass extinction: National Academy of Sciences Proceedings, v. 108, p. 17631–17634, doi:10.1073/pnas.1106039108.

Burgess, S.D., and Bowring, S.A., 2015, High-precision geochronology confirms voluminous magmatism before, during, and after Earth's most severe extinction: Science Advances, v. 1, p. 1–14, doi:10.1126/sciadv.1500470.

Burgess, S.D., Bowring, S., and Shen, S.Z., 2014, High-precision timeline for Earth's most severe extinction: National Academy of Sciences Proceedings, v. 111, p. 3316–3321, doi:10.1073/pnas.1317692111 (erratum available at http://dx.doi.org/10.1073/pnas.1403228111).

Cao, C.Q., Love, G.D., Hays, L.E., Wang, W., Shen, S.Z., and Summons, R.E., 2009, Biogeochemical evidence for euxinic oceans and ecological disturbance presaging the end-Permian mass extinction event: Earth and Planetary Science Letters, v. 281, p. 188–201, doi:10.1016/j.epsl.2009.02.012.

Chen, H., Savage, P.S., Teng, F.-Z., Helz, R.T., and Moynier, F., 2013, Zinc isotope fractionation during magmatic differentiation and the isotopic composition of the bulk Earth: Earth and Planetary Science Letters, v. 369–370, p. 34–42, doi:10.1016/j.epsl.2013.02.037.

Conway, T.M., and John, S.G., 2014, The biogeochemical cycling of zinc and zinc isotopes in the North Atlantic Ocean: Global Biogeochemical Cycles, v. 28, p. 1111–1128, doi:10.1002/2014GB004862.

Erwin, D.H., 2006, Extinction: How life on Earth nearly ended 250 million years ago: Princeton, New Jersey, Princeton University Press, 320 p.

Fujii, T., Moynier, F., Pons, M.L., and Albarède, F., 2011, The origin of Zn isotope fractionation of sulfides: Geochimica et Cosmochimica Acta, v. 75, p. 7632–7643, doi:10.1016/j.gca.2011.09.036.

Garbelli, C., Angiolini, L., and Shen, S.Z., 2017, Biomineralization and global change: A new perspective for understanding the end-Permian extinction: Geology, v. 45, p. 19–22, doi:10.1130/G38430.1.

Grice, K., Cao, C.Q., Love, G.D., Bottcher, M.E., Twitchett, R.J., Grosjean, E., Summons, R.E., Turgeon, S.C., Dunning, W., and Jin, Y.G., 2005, Photic zone euxinia during the Permian-Triassic superanoxic event: Science, v. 307, p. 706–709, doi:10.1126/science.1104323.

Hendry, K.R., and Andersen, M.B., 2013, The zinc isotopic composition of siliceous marine sponges: Investigating nature's sediment traps: Chemical Geology, v. 354, p. 33–41, doi:10.1016/j.chemgeo.2013.06.025.

Jin, Y.G., Shen, S.Z., Henderson, C.M., Wang, X.D., Wang, W., Wang, Y., Cao, C.Q., and Shang, Q.H., 2006, The Global Stratotype Section and Point (GSSP) for the boundary between the Capitanian and Wuchiapingian Stage (Permian): Episodes, v. 29, p. 253–262.

Joachimski, M.M., Lai, X.L., Shen, S.Z., Jiang, H.S., Luo, G.M., Chen, B., Chen, J., and Sun, Y.D., 2012, Climate warming in the latest Permian and the Permian-Triassic mass extinction: Geology, v. 40, p. 195–198, doi:10.1130/G32707.1.

Kershaw, S., et al., 2012, Microbialites and global environmental change across the Permian-Triassic boundary: A synthesis: Geobiology, v. 10, p. 25–47, doi: 10.1111/j.1472-4669.2011.00302.x.

Korte, C., and Kozur, H.W., 2010, Carbon-isotope stratigraphy across the Permian-Triassic boundary: A review: Journal of Asian Earth Sciences, v. 39, p. 215–235, doi:10.1016/j.jseaes.2010.01.005.

Kunzmann, M., Halverson, G.P., Sossi, P.A., Raub, T.D., Payne, J.L., and Kirby, J., 2013, Zn isotope evidence for immediate resumption of primary productivity after snowball Earth: Geology, v. 41, p. 27–30, doi:10.1130/G33422.1.

Little, S.H., Vance, D., Walker-Brown, C., and Landing, W.M., 2014, The oceanic mass balance of copper and zinc isotopes, investigated by analysis of their inputs, and outputs to ferromanganese oxide sediments: Geochimica et Cosmochimica Acta, v. 125, p. 673–693, doi:10.1016/j.gca.2013.07.046.

Maréchal, C.N., Nicolas, E., Douchet, C., and Albarède, F., 2000, Abundance of zinc isotopes as a marine biogeochemical tracer: Geochemistry, Geophysics, Geosystems, v. 1, 1015, doi:10.1029/1999GC000029.

Payne, J.L., Turchyn, A.V., Paytan, A., DePaolo, D.J., Lehrmann, D.J., Yu, M.Y., and Wei, J.Y., 2010, Calcium isotope constraints on the end-Permian mass extinction: National Academy of Sciences Proceedings, v. 107, p. 8543–8548, doi:10.1073/pnas.0914065107.

Peel, K., Weiss, D., and Sigg, L., 2009, Zinc isotope composition of settling particles as a proxy for biogeochemical processes in lakes: Insights from the eutrophic Lake Greifen, Switzerland: Association for the Sciences of Limnology and Oceanography, v. 54, p. 1699–1708, doi:10.4319/lo.2009.54.5.1699.

Pichat, S., Douchet, C., and Albarède, F., 2003, Zinc isotope variations in deep-sea carbonates from the eastern equatorial Pacific over the last 175 ka: Earth and Planetary Science Letters, v. 210, p. 167–178, doi:10.1016/S0012-821X(03)00106–7.

Reichow, M.K., et al., 2009, The timing and extent of the eruption of the Siberian Traps large igneous province: Implications for the end-Permian environmental crisis: Earth and Planetary Science Letters, v. 277, p. 9–20, doi:10.1016/j.epsl.2008.09.030.

Shen, S.Z., et al., 2011, Calibrating the end-Permian mass extinction: Science, v. 334, p. 1367–1372, doi:10.1126/science.1213454.

Shen, S.Z., et al., 2013, High-resolution $\delta^{13}C_{carb}$ chemostratigraphy from latest Guadalupian through earliest Triassic in south China and Iran: Earth and Planetary Science Letters, v. 375, p. 156–165, doi:10.1016/j.epsl.2013.05.020.

Shiller, A.M., and Boyle, E., 1985, Dissolved zinc in rivers: Nature, v. 317, p. 49–52, doi:10.1038 /317049a0.

Sun, Y.D., Joachimski, M.M., Wignall, P.B., Yan, C.B., Chen, Y.L., Jiang, H.S., Wang, L.N., and Lai, X.L., 2012, Lethally hot temperatures during the Early Triassic greenhouse: Science, v. 338, p. 366–370, doi:10.1126/science.1224126.

Vance, D., Little, S.H., Archer, C., Cameron, V., Andersen, M.B., Rijkenberg, M.J.A., and Lyons, T.W., 2016, The oceanic budgets of nickel and zinc isotopes: The importance of sulfidic environments as illustrated by the Black Sea: Philosophical Transactions of the Royal Society A: Mathematical, Physical and Engineering Sciences, v. 374, p. 1-26, doi:10.1098/rsta.2015.0294.

Whiteside, J.H., and Grice, K., 2016, Biomarker records associated with mass extinction events: Annual Review of Earth and Planetary Sciences, v. 44, p. 581–612, doi:10.1146/annurev-earth-060115-012501.

Wu, H.C., Zhang, S.H., Hinnov, L.A., Jiang, G.Q., Feng, Q.L., Li, H.Y., and Yang, T.S., 2013, Time-calibrated Milankovitch cycles for the late Permian: Nature Communications, v. 4, p. 2452–2459, doi:10.1038/ncomms3452.

Yin, H.F., Zhang, K.X., Tong, J.N., Yang, Z.Y., and Wu, S.B., 2001, The Global Stratotype Section and Point (GSSP) of the Permian-Triassic boundary: Episodes, v. 24, p. 102–114.

Ziegler, A.M., Hulver, M.L., and Rowley, D.B., 1997, Permian world topography and climate, *in* Martini, I.P., ed., Late glacial and postglacial environmental changes—Quaternary, Carboniferous-Permian and Proterozoic: New York, Oxford University Press, p. 111–146.

Manuscript received 30 September 2016
Revised manuscript received 17 December 2016
Manuscript accepted 23 December 2016

Printed in USA